Hindawi
International Journal of Antennas and Propagation
Volume 2020, Article ID 8881317, 17 pages
https://doi.org/10.1155/2020/8881317

Research Article

Design of a Broadband Radome-Enclosed Dual-Polarization Antenna Array Covering Sub-6 GHz Band with Differential Feeding

Zhirong An and Mang He

School of Information and Electronics, Beijing Institute of Technology, Beijing 100081, China

Correspondence should be addressed to Mang He; hemang@bit.edu.cn

Received 18 September 2020; Revised 3 November 2020; Accepted 9 November 2020; Published 1 December 2020

Academic Editor: Giorgio Montisci

A differentially fed dual-polarized antenna with low cross-polarization is proposed for sub-6 GHz applications. The main patch is fed through two pairs of symmetrical ports, and annular-ring slits are etched around the feedings. The broadband 180° phase shifter provides a stable differential feeding structure, and a 1 mm thick radome with a parasitic patch printed on its inner surface is utilized to expand the impedance bandwidth. The impedance bandwidth of the proposed antenna ranges from 3.3 to 6.0 GHz, covering the entire sub-6 GHz band. The 4-element antenna array features low profile, wide bandwidth, low cross-polarization level, and stable gain over the entire operating band. The prototype of the antenna array is fabricated and measured, and the design is well validated by experimental results.

1. Introduction

The 3rd Generation Partnership Project (3GPP) has recommended the sub-6 GHz bands (3.3–4.2 GHz and 4.4–5 GHz) [1, 2] and mm-wave frequency bands (24.25–29.5 GHz) [3] as the 5G New Radio (NR) bands. Compared with mm-wave band, sub-6 GHz band has the advantages of less signal attenuation, long transmission distance, and being not easy to be blocked. Therefore, the sub-6 GHz band is more suitable to ensure outdoor signal coverage. On this basis, in order to make full use of spectrum resource, polarization diversity technology has been widely used. As a transmitting or receiving antenna in these communication systems, dual-polarized antenna design is preferred, since it can increase the channel capacity and reduce the multipath fading effect. Meanwhile, low cross-polarization level and high isolation between feeding ports are required, because multiple-input ports are necessary to achieve the dual polarization. Thus, a dual-polarized antenna/array working at sub-6 GHz band with low cross-polarization and high isolation is worth studying.

There have been many antenna designs reported for sub-6 GHz applications in recent years [4–21], which can be divided into two types approximately: crossed-dipole antennas and patch antennas. The crossed-dipole antennas usually have the advantage of wide bandwidth; however, due to the limit of the perfect electric conductor (PEC) reflector, these antennas usually have a relatively high profile around $0.25\lambda_0$ (λ_0 is the free-space wavelength at the center frequency). In [5], a low profile differentially fed dual-polarization antenna is proposed for 5G microcell communications. By introducing an artificial magnetic conductor (AMC) reflector that is composed of annular patches, the profile can be reduced to $0.13\lambda_0$. However, the AMC structure increases the cost of fabrication, which limits mass production. Meanwhile, patch antennas have also received extensive attention due to its advantages of low profile and low cost. In [17], a differentially driven dual-polarized patch antenna that utilizes the intersected open-loop resonators is proposed for wireless communication systems. In [19], a dual-band dual-polarization filtering antenna is achieved by employing the coupled resonator

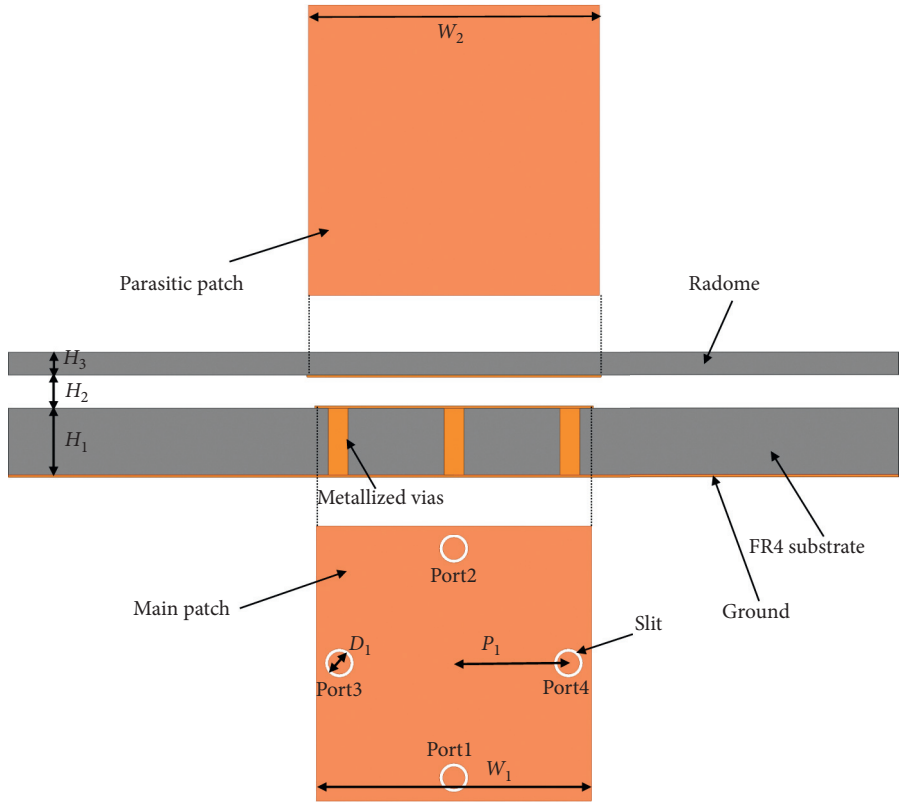

Figure 1: Configuration of the antenna element.

Table 1: Optimum dimensions of the antenna element (unit: mm).

Parameter	W_1	W_2	D_1	P_1	H_1	H_2	H_3
Values	12.5	13.2	1	5.2	3	1.5	1

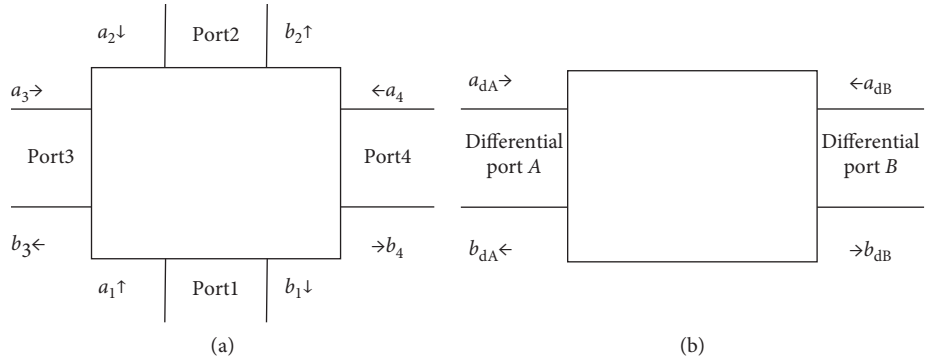

Figure 2: Four-port network and differential two-port network model of the antenna element.

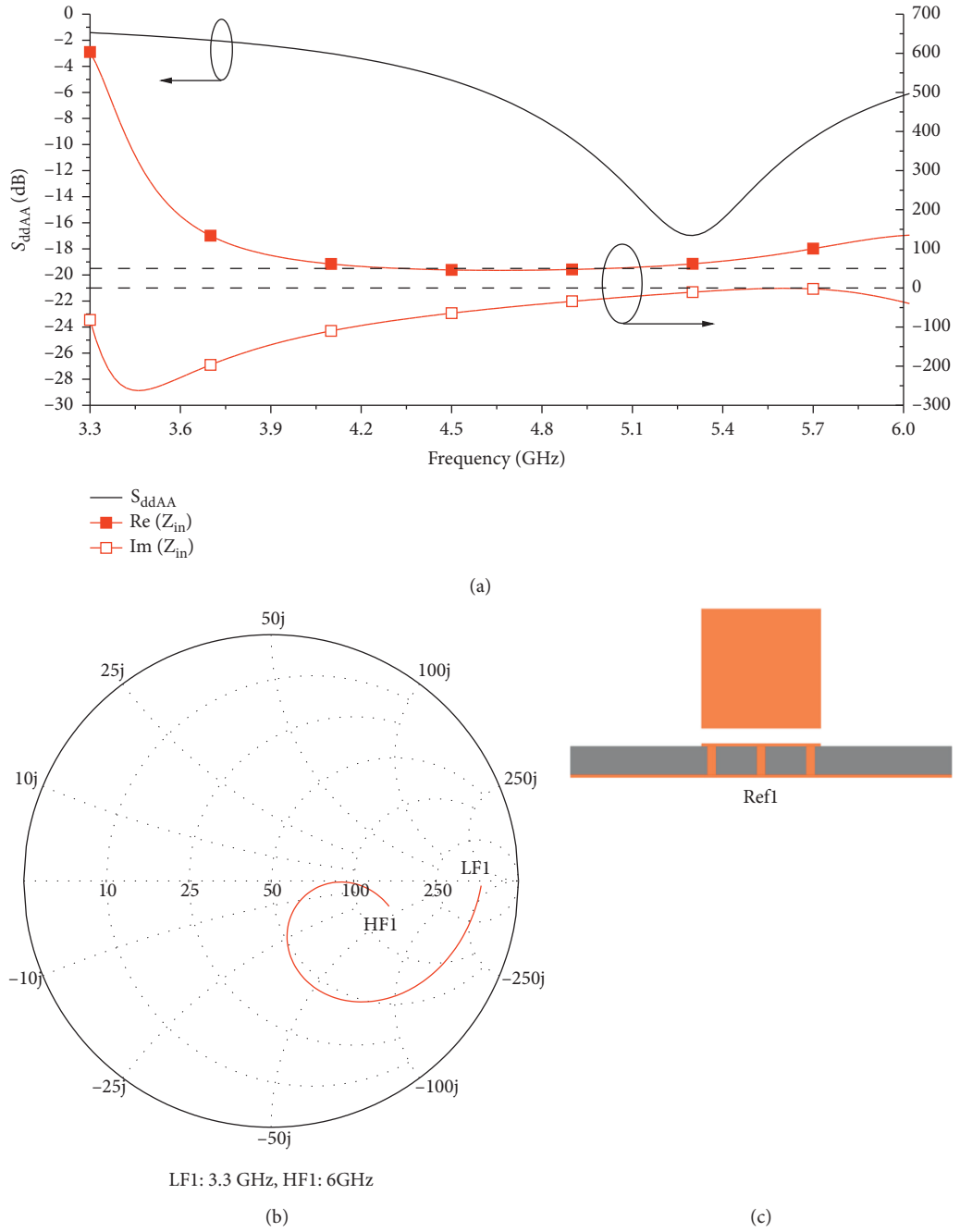

Figure 3: Simulated $(S)_{ddAA}$, Z_{in}, and Smith chart of the single-layer patch antenna.

technique. However, due to the low profile and planar configuration, patch antennas normally face the problem of limited bandwidth, which makes it difficult to meet the bandwidth requirement for sub-6 GHz applications. In [20], combined with differential feeding scheme, a dual-polarized antenna achieves a wider bandwidth of 26% (3–3.9 GHz) with low profile of $0.13\lambda_0$; however, this bandwidth is still not adequate to cover the entire sub-6 GHz band.

In this paper, the design of a broadband dual-polarized antenna that works stably throughout the entire sub-6 GHz band is proposed. Not only has the effect of the radome been taken into consideration in the design, but also the radome structure is utilized to expand the impedance bandwidth of the antenna. This integrated design results in a very wide bandwidth ranging from 3.3 to 6 GHz. Owing to the differential feeding technique, the

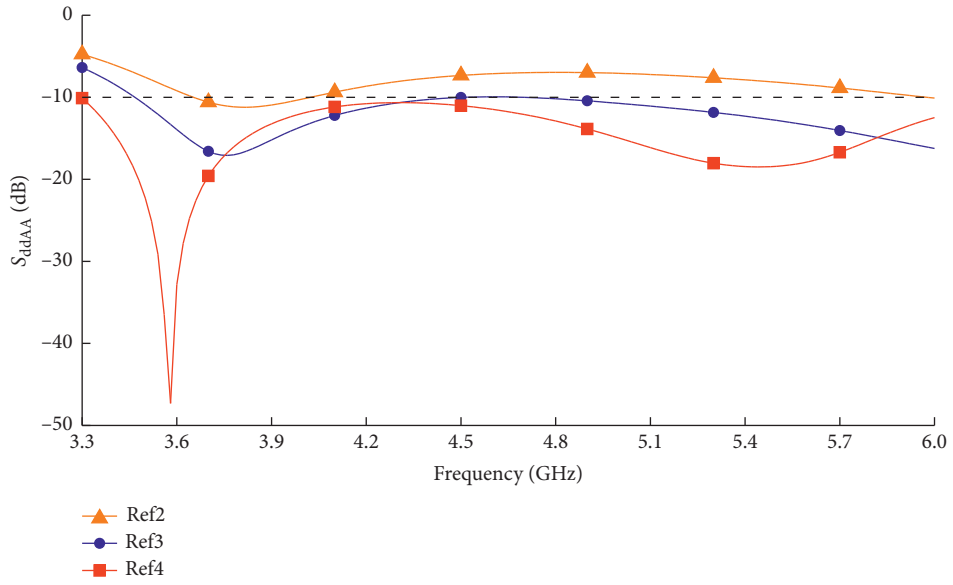

(a)

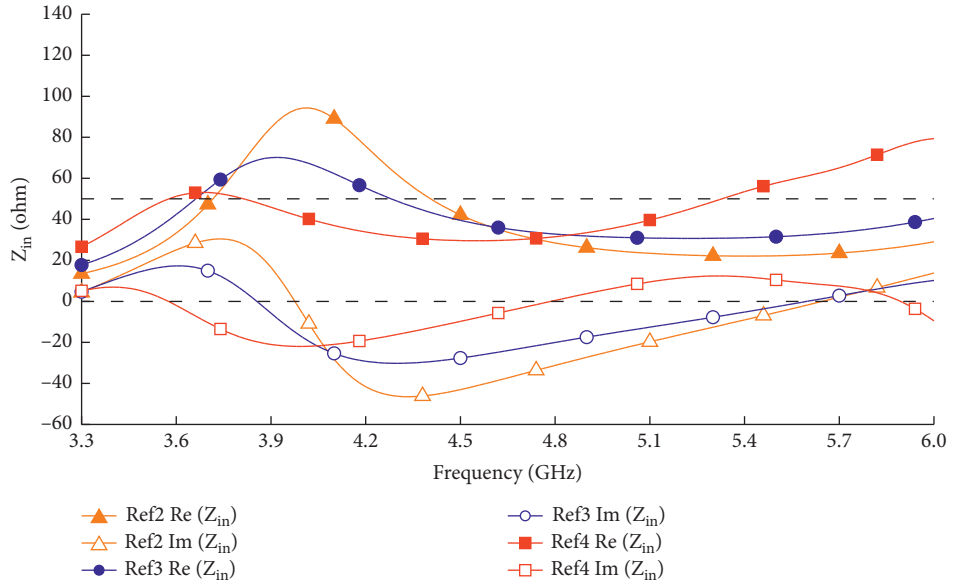

(b)

Figure 4: Continued.

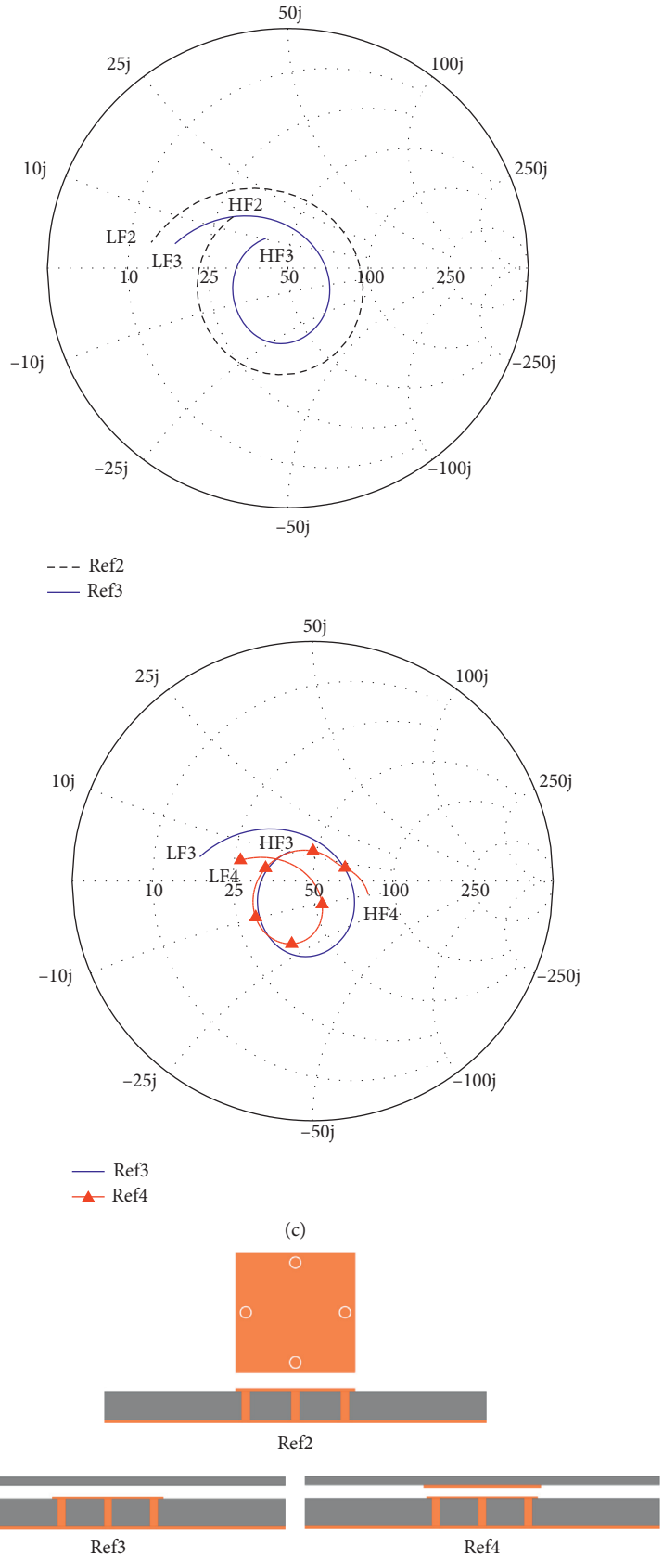

Figure 4: Simulated $(S)_{ddAA}$, Z_{in}, and Smith chart of different antennas.

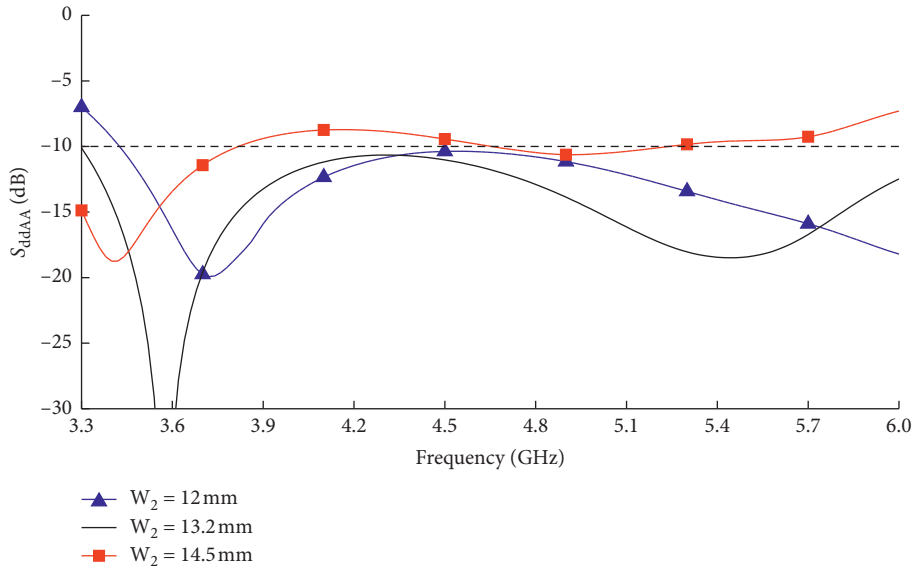

(a)

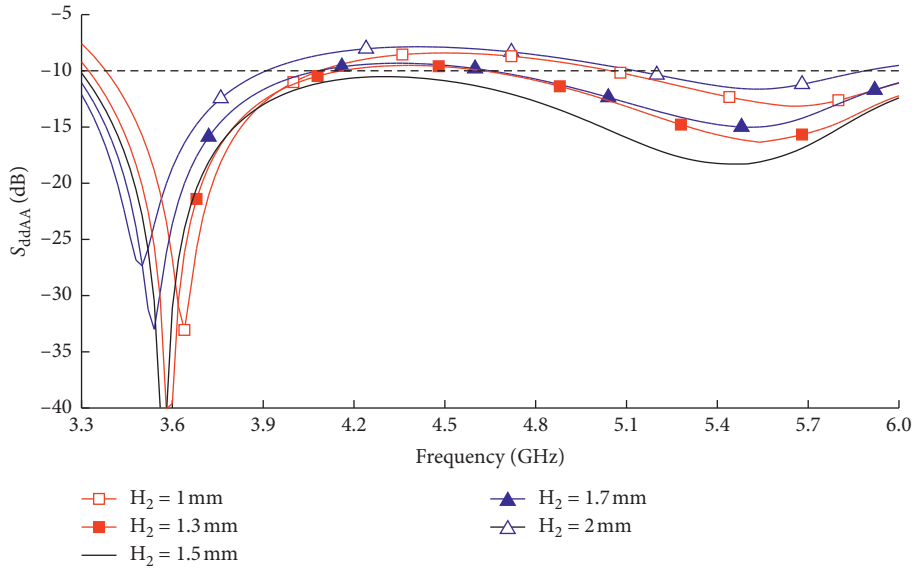

(b)

Figure 5: Continued.

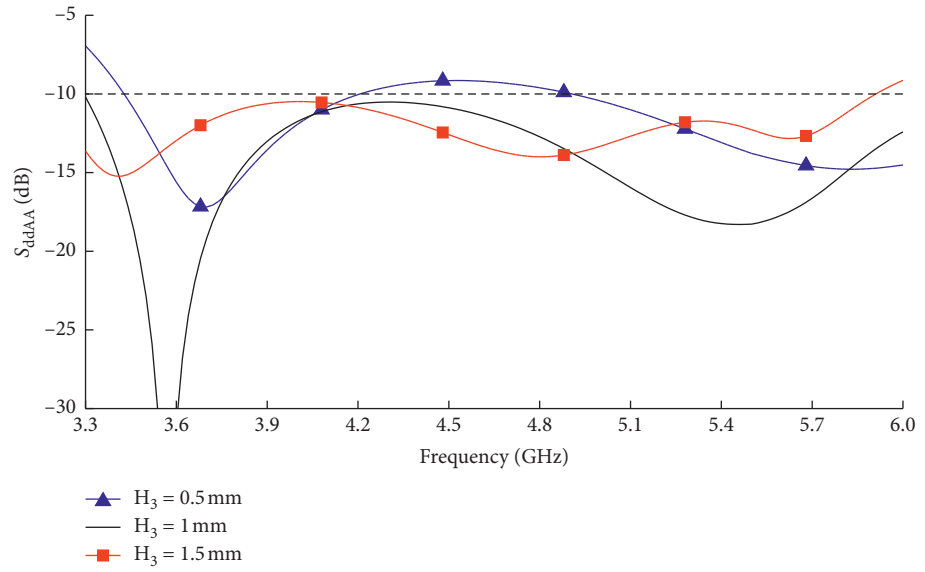

(c)

Figure 5: Parametric studies of the proposed antenna by changing the values of (a) W_2, (b) H_2, and (c) H_3.

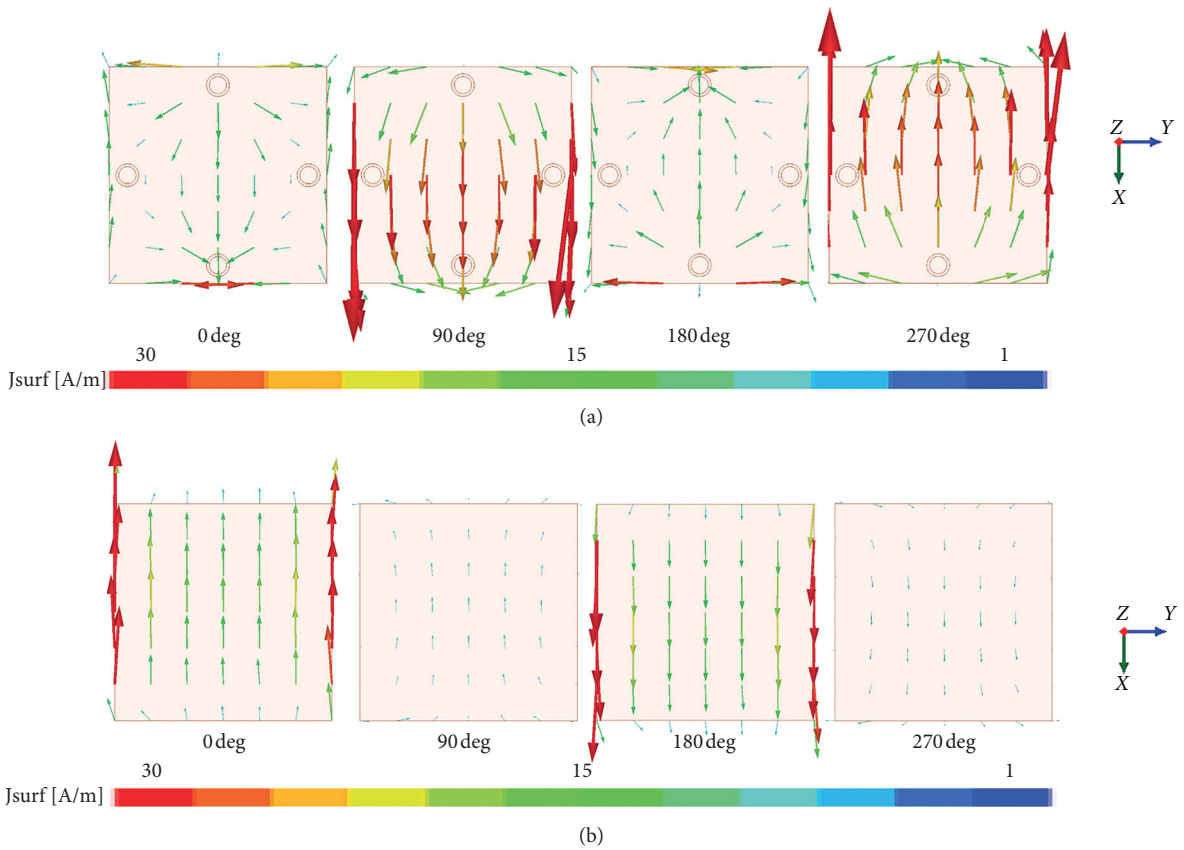

(a)

(b)

Figure 6: Current distributions on the main patch and the parasitic patch when port A is fed differentially: (a) main patch and (b) parasitic patch.

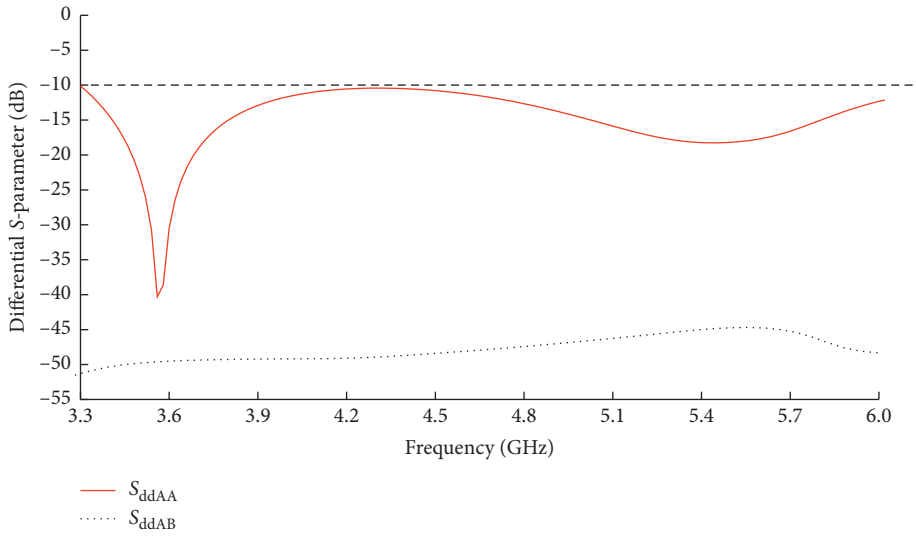

Figure 7: Simulated differential (S)-parameters of proposed antenna.

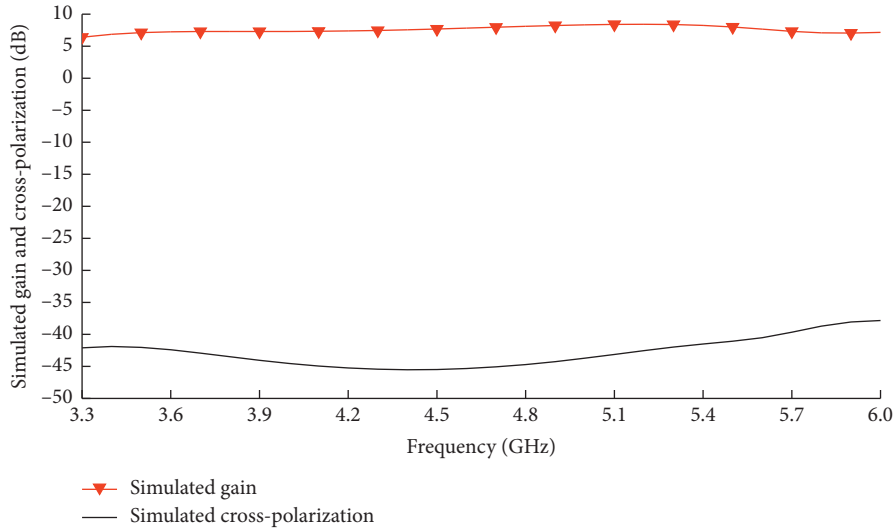

Figure 8: Simulated gain and cross-polarization of the antenna at the broadside direction.

1×4 antenna array possesses low cross-polarization, high isolation, stable gain, and radiation pattern within the entire frequency band.

2. Antenna Design

2.1. Antenna Element. Figure 1 shows the geometry of the antenna element. The main radiator is a square patch that is printed on an FR4 substrate ($\varepsilon_r = 4.4$, $\tan\delta = 0.02$) with the thickness H_1. The patch has the side length of W_1 and is differentially fed through four ports (named ports 1 to 4). Each port is P_1 distant from the patch's center and is connected to the ground via a metallized via hole. In addition, an annular-ring slit with the inner diameter D_1 is etched from the patch around each via hole for convenient tuning of the antenna's input impedance. Above the main patch, an FR4 slab with the thickness H_3 is used as the radome to protect the antenna from outside environments. To maintain a low profile of the entire antenna structure, the space H_2 between the radome and the main radiator should

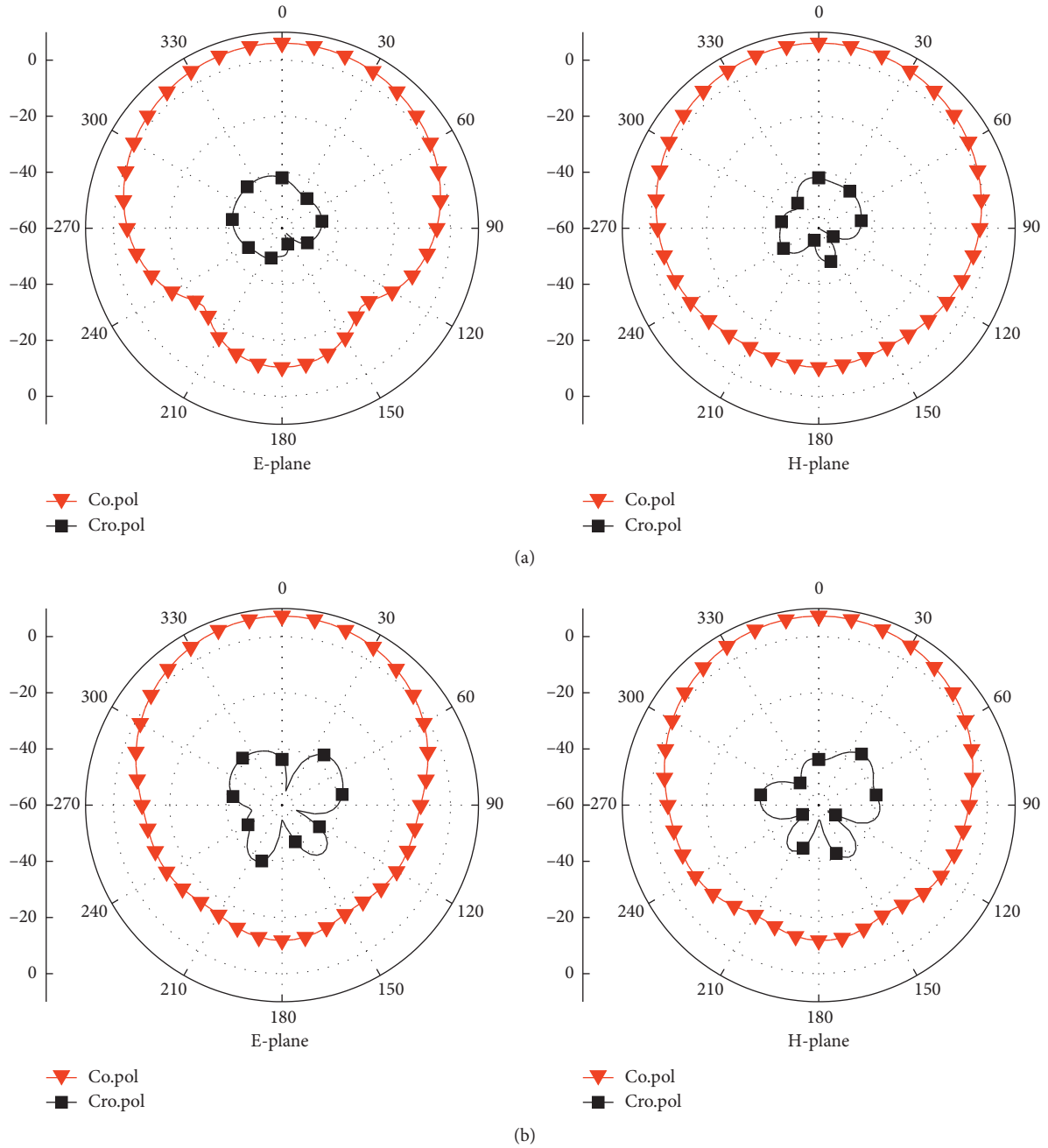

Figure 9: Simulated radiation patterns of the antenna at two different frequencies. (a) 3.5 GHz; (b) 5 GHz.

not be large. Therefore, due to the close proximity between them, the radome has significant effects on the radiation performance of the main patch. However, in this design, we utilize the positive role of the radome and print a parasitic square patch with the side length W_2 on the inner surface of it to build a stacked patch structure for bandwidth expansion. Through exhaustive parametric study, the optimum dimensions of the antenna element are obtained and listed in Table 1 for reference.

2.2. Working Principle. Since the antenna is fed differentially through two pairs of symmetrical ports, the proposed antenna is a single-ended four-port network, as shown in Figure 2(a). According to the definition of S-parameters, we have

$$[b] = [S][a]. \quad (1)$$

At the same time, when ports 1 and 2 are excited with equal magnitude and 180° phase difference, they can be

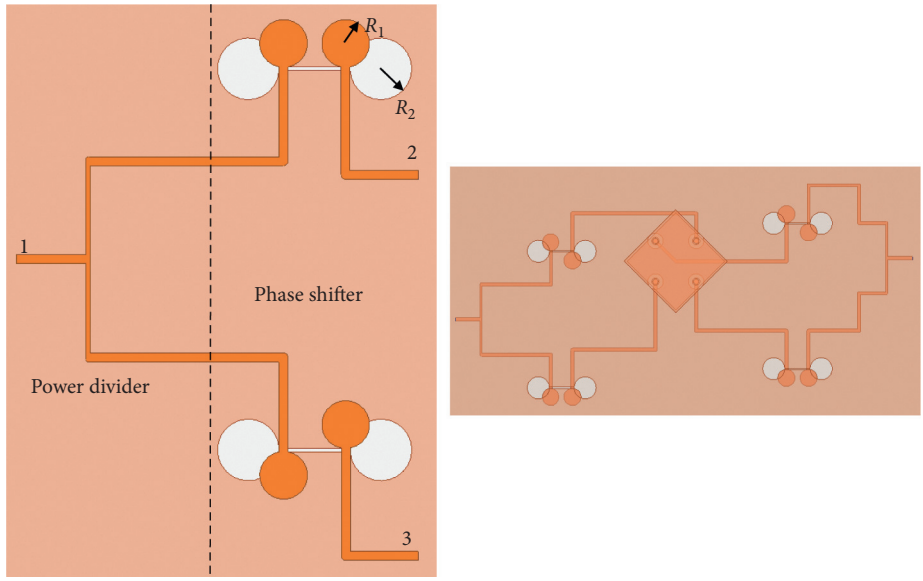

Figure 10: Configuration of the feeding network.

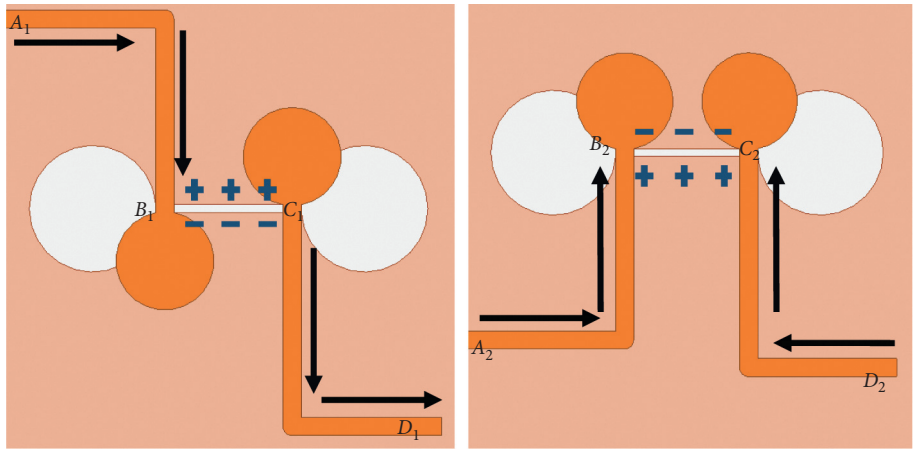

Figure 11: Distribution of current and electric field of the feeding network.

considered as a pair of differential port (named port A) [22]. Similarly, ports 3 and 4 can also be regarded as the differential port B. As defined in [22], the antenna is actually a two-port differential network, as shown in Figure 2(b). At this time, we have

$$\begin{bmatrix} b_{dA} \\ b_{dB} \end{bmatrix} = \begin{bmatrix} S_{ddAA} & S_{ddAB} \\ S_{ddBA} & S_{ddBB} \end{bmatrix} \cdot \begin{bmatrix} a_{dA} \\ a_{dB} \end{bmatrix}, \tag{2}$$

where

$$\begin{aligned} b_{dA} &= b_1 - b_2, \\ b_{dB} &= b_3 - b_4, \\ a_{dA} &= a_1 - a_2, \\ a_{dB} &= a_3 - a_4. \end{aligned} \tag{3}$$

Considering the differential port A, when ports 1 and 2 are differentially excited while port 3 and 4 are connected to 50 Ω loadings, the differential S-parameters can be defined:

$$\begin{aligned} S_{ddAA} &= \frac{b_{dA}}{a_{dA}}\Big|_{a_{dB}=0} = \frac{1}{2}(S_{11} - S_{12} - S_{21} + S_{22}), \\ S_{ddBA} &= \frac{b_{dB}}{a_{dA}}\Big|_{a_{dB}=0} = \frac{1}{2}(S_{31} - S_{32} - S_{41} + S_{42}). \end{aligned} \tag{4}$$

Similarly, we get

$$\begin{aligned} S_{ddAB} &= \frac{b_{dA}}{a_{dB}}\Big|_{a_{dA}=0} = \frac{1}{2}(S_{13} - S_{14} - S_{23} + S_{24}), \\ S_{ddBA} &= \frac{b_{dB}}{a_{dB}}\Big|_{a_{dA}=0} = \frac{1}{2}(S_{33} - S_{34} - S_{43} + S_{44}). \end{aligned} \tag{5}$$

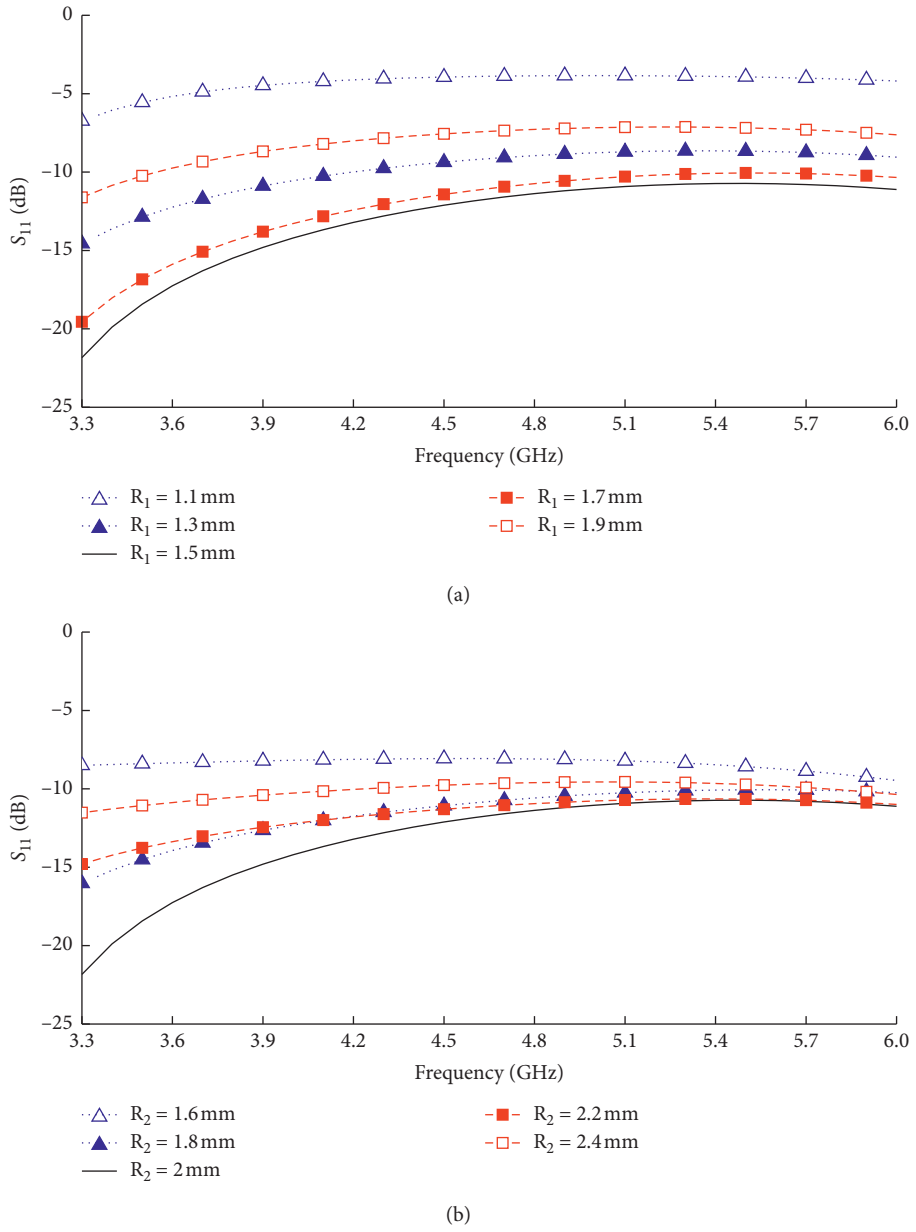

Figure 12: Parametric studies of the feeding network by changing the values of (a) R_1 and (b) R_2.

On the basis of the above discussion, the antenna design can be carried out as follows: First, only single-layer patch antenna is considered, as shown in Figure 3, Ref1. The length of the main patch is $W_1 = 12.5$ mm, which is about 1/2 λ_g at 5.3 GHz (λ_g is the guided wavelength). On this basis, annular-ring slits are etched around the feedings [23], as shown in Figure 4, Ref2. The annular-ring slits change the impedance characteristics of the feeding point, causing the input impedance curve of the antenna surrounding the origin on the Smith chart. Next, a radome is added above the main patch, as shown in Figure 4, Ref3. As shown in Figures 4(b) and 4(c), the radome has the effect of impedance matching, thereby improving the impedance bandwidth of the antenna. As shown in Figure 4(a), the antenna shown in Ref3 is still poorly matched at low frequencies (3.3–3.5 GHz). For this reason, a large-sized parasitic patch is printed on the lower surface of the radome, thereby improving

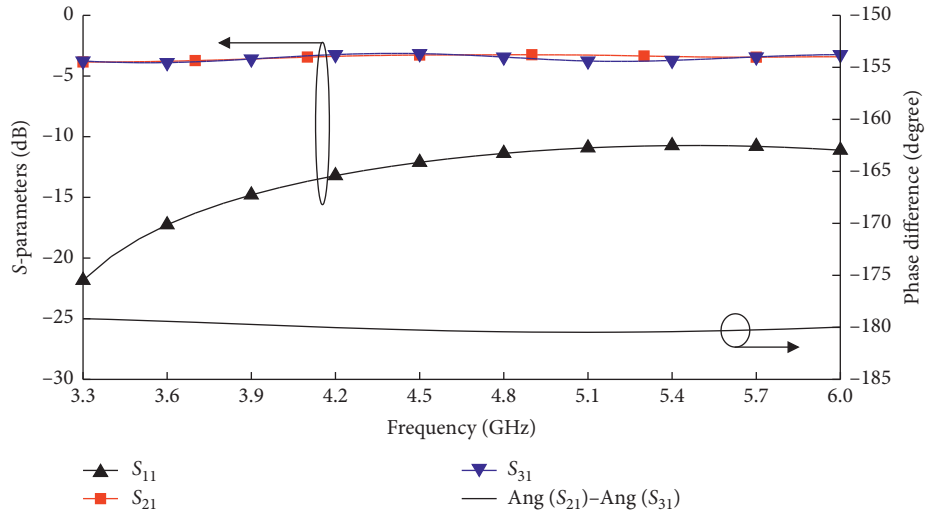

Figure 13: Simulated (S)-parameters and phase difference of the feeding network.

the impedance matching at low frequencies, which makes the antenna cover the entire sub-6 GHz band. The parametric studies of the antenna parameters are shown in Figure 5.

The current distribution on the patch is relatively consistent throughout the entire frequency band, and no high-order modes were generated. Taking 5 GHz as an example, the current distribution is shown in Figure 6. When port A is differentially fed, the current direction is along the x-direction; and, symmetrically, when port B is differentially fed, the current direction is along the y-direction. Thereby, two orthogonally polarized waves are generated. Meanwhile, the proposed antenna has a high port isolation, as shown in Figure 7. Because the antenna structure is symmetrical, S_{31} equals S_{41} and S_{32} is equal to S_{42} according to the network theory. Thus, S_{ddBA} should be zero from equation (4), which means that high isolation is a natural result of the differential feeding scheme. Figure 6 can also be used to illustrate this point, in which when the differential port A is fed, the current near ports 3 and 4 is completely symmetrical. This indicates that the potential difference between the two ports is zero, and no current will flow into ports 3 and 4, which leads to a high isolation between two differential ports.

Figure 8 shows the simulated gain and cross-polarization level of the antenna at the broadside direction. Due to the differential feeding, on the two half patches, the direction of the currents that are orthogonal to the main currents is opposite, so the cross-polarization radiation can be very low. Within the entire sub-6 GHz band, the cross-polarization level is less than −45 dB. The simulated radiation pattern of the antenna at two typical frequencies in the 5G NR band is shown in Figure 9, and the maximum cross-polarization is observed to be less than −36 dB within the space of solid angle $\theta \leq 60^{\circ}$.

2.3. Feeding Network. As seen in the last subsection, the antenna will maintain very stable performance if the feeding provides ideal differential signal. Therefore, it is extremely important for the feeding network to output two stable signals with equal magnitude and reverse phase within a very wide band that can cover the entire sub-6 GHz frequencies. In this design, we use the feeding network that is shown in Figure 10. The network consists of a simple T-type power divider with one phase shifter cascading on each of the two output branches. The phase shifter adopts a transition structure from microstrip line to ground slot [24]. As shown in Figure 11, the current transmits along the microstrip line (A_1–B_1 or A_2–B_2) and then couples to the slot through a microstrip-slot transition structure at point B_1 or B_2 and then transmits along the slot (B_1–C_1 or B_2–C_2) until it is coupled to the microstrip line at point C_1 or C_2. Since the coupling direction is opposite at C_1 and C_2 with reference to the direction of electric field (marked as + and − in Figure 11), 180° phase difference is introduced between the two branches. Moreover, the total length of the two branches is approximately identical (A_1–D_1 and A_2–D_2), so, compared with traditional phase shifters, the output signals at the end of two branches (i.e., at the points D_1 and D_2) have the same magnitude and 180° phase difference almost independent of frequency. In addition, the impedance matching of the structure can be finely tuned by changing the radius of the circular stub (R_1 and R_2), as shown in Figure 12. The simulated S-parameters of the feeding network are shown in Figure 13. It is seen that the transmission loss ranges from

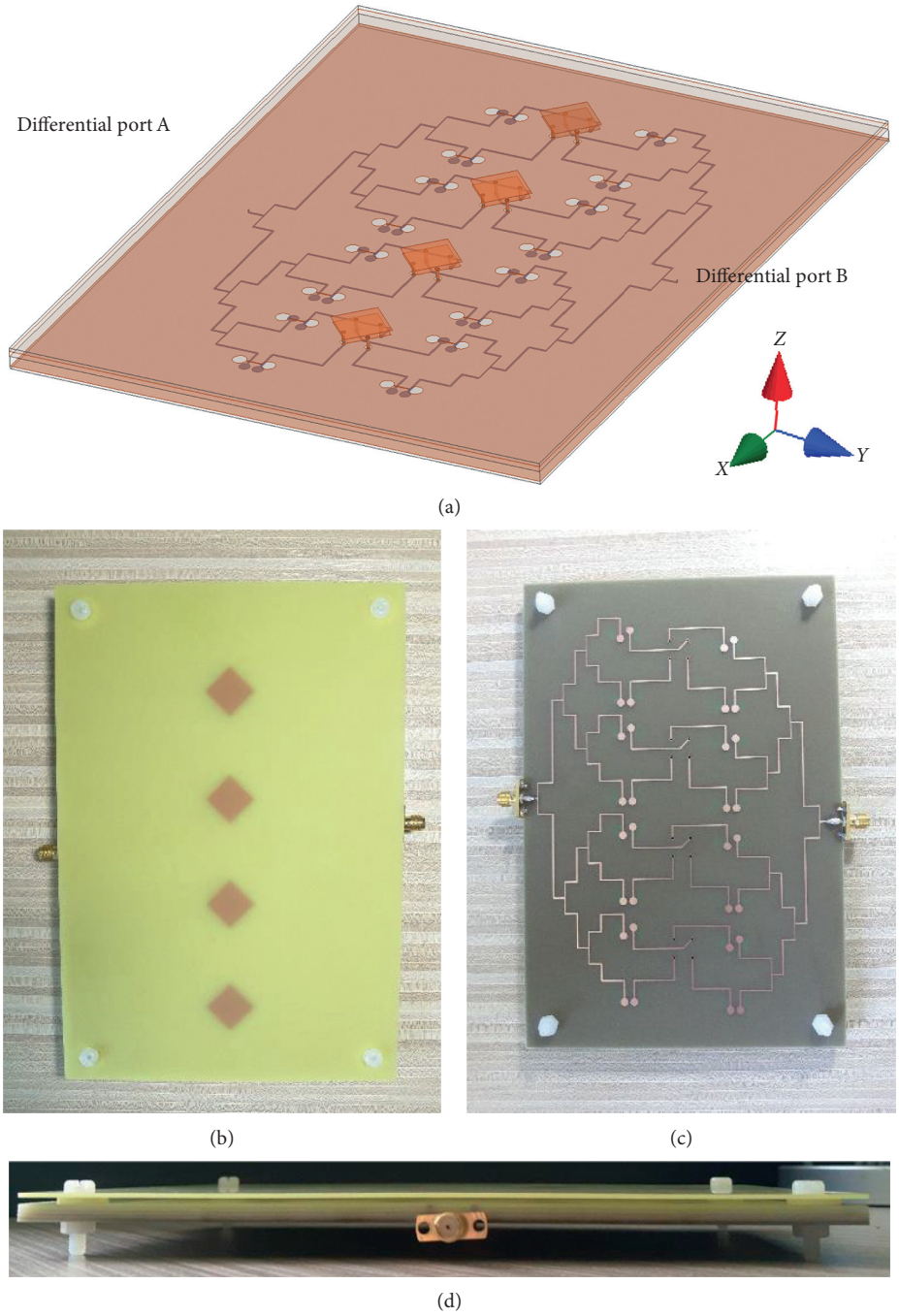

Figure 14: Simulation model and fabricated prototype of the 1×4 antenna array. (a) Simulation model, (b) top view, (c) back view, and (d) side view of the fabricated prototype.

−3.60 to −3.13 dB, which is mainly due to the relatively large dielectric loss of the low-cost FR4 substrate ($\tan\delta = 0.02$). Within the entire frequency band, the return loss is better than 12 dB and the phase difference of the two output ports is $180^\circ \pm 0.8^\circ$, which shows very stable broadband phase shift performance.

3. Antenna Array and Results

As shown in Figure 14, a 4-element linear array is designed, and the prototype is fabricated and measured for possible use in sub-6 GHz applications. The interelement spacing is 40 mm, corresponding to $0.62\lambda_0$ (λ_0 is the free-space

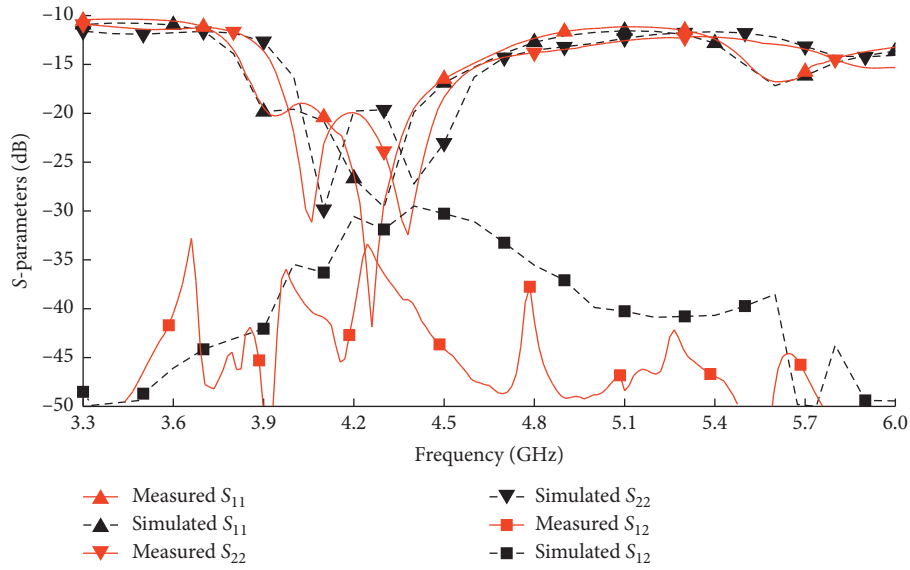

Figure 15: Simulated and measured (S)-parameters of the antenna array.

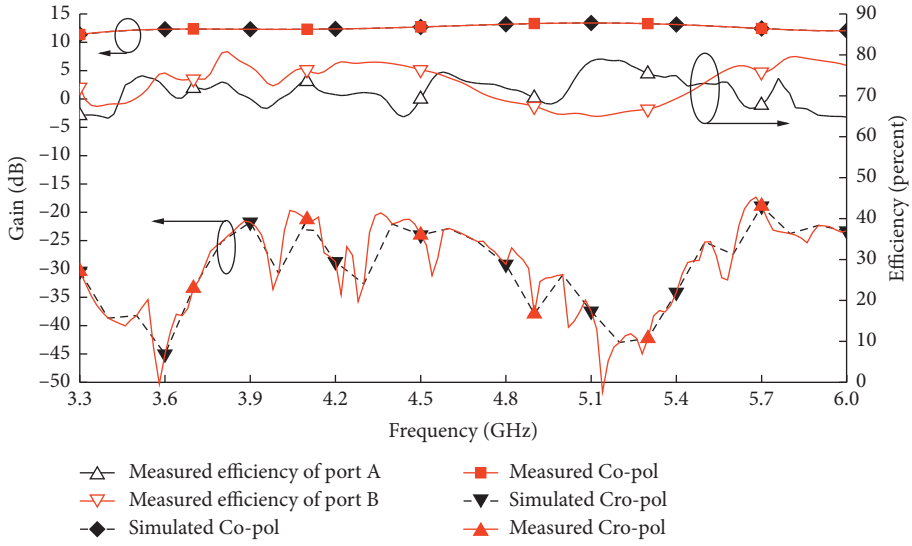

Figure 16: Simulated and measured gain and efficiency of the antenna array.

wavelength at the center frequency 4.65 GHz of the sub-6 GHz band). All the measurements are carried out using the multiprobe wireless communication test system Ray-Zone 1800. Figure 15 shows the simulated and measured S-parameters of the antenna array. It is seen that the measured results agree well with the simulated ones, and throughout the 3.3–6.0 GHz frequency range the measured reflection coefficients at the two feeding ports are less than −10 dB and the port isolation is greater than 33 dB. The simulated and measured peak gain and total efficiency of the array, when only the differential port A is fed and the other port is connected to a matched load, are shown in Figure 16. The measured cross-polarization is lower than −30 dB within the entire frequency band. Compared to the simulation results of the antenna element, both the cross-polarization level and the port isolation are slightly deteriorated due to the feeding network because it introduces asymmetry between two ports in some extent, which may raise the cross-polarization radiation and reduce the port isolation. It is also found in Figure 16 that the total efficiency of the antenna

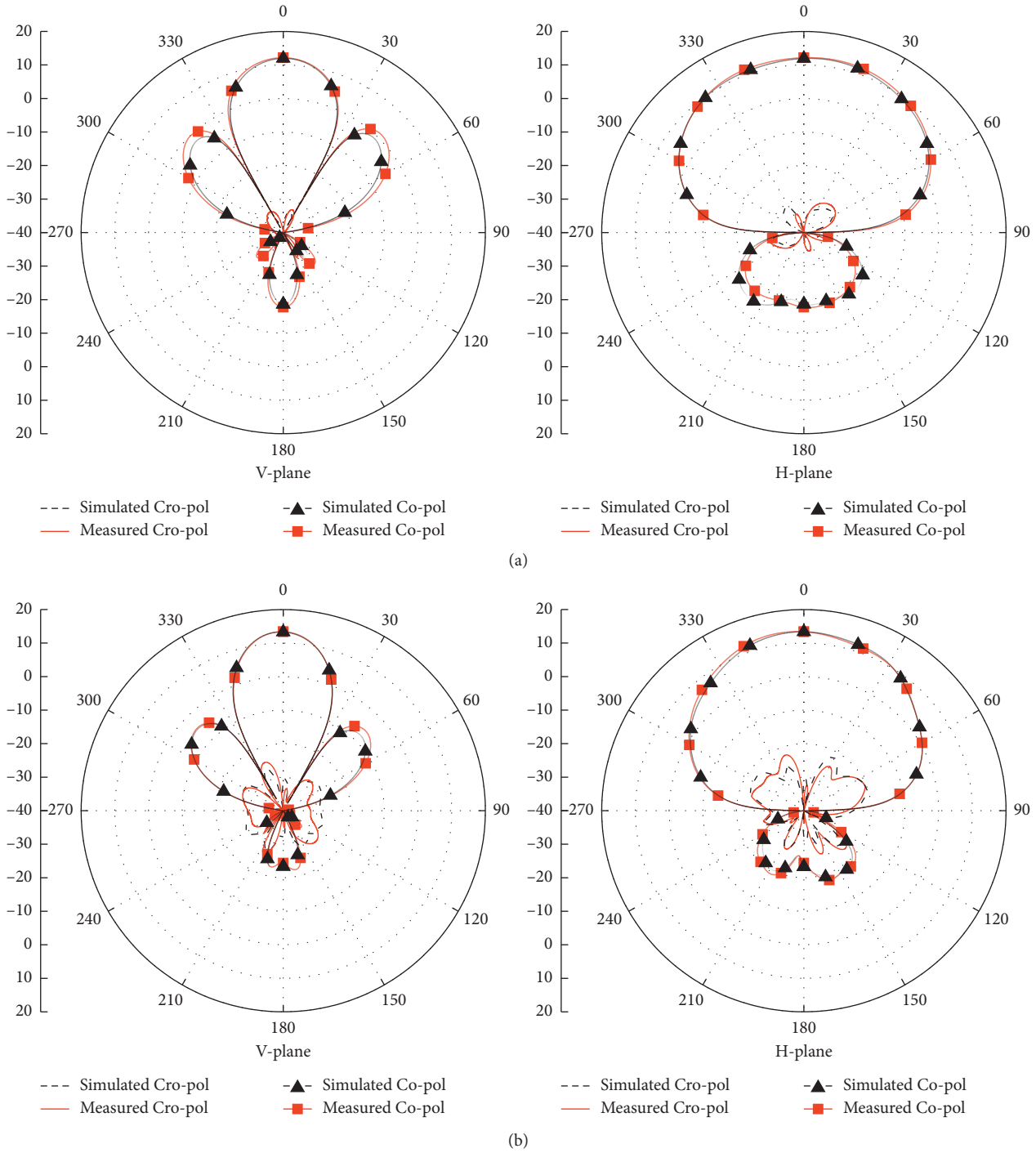

Figure 17: Simulated and measured radiation patterns of the antenna array at (a) 3.5 GHz and (b) 5.0 GHz.

maintains above 65% within the entire operating frequency band despite the use of low-cost FR4 substrate with large dielectric loss. Figure 17 shows the radiation patterns of the proposed array at two different frequencies 3.5 and 5.0 GHz when only the differential port A is fed, in which the xoz-plane is defined as the V-plane (vertical plane) and the yoz-plane is defined as the H-plane (horizontal plane). It is clear that the radiation pattern is stable and the cross-polarization level is lower than −35 dB at the two frequencies.

Table 2 shows comparison of the measured performance of the proposed antenna array with the existing works. Compared with the previous designs, the proposed antenna has the widest bandwidth from 3.3 to 6.0 GHz, which can cover the entire sub-6 GHz band. It also has the lowest cross-polarization level, which is −30 dB. At the same time, it has acceptable gain and efficiency compared with [5, 19]. The proposed antenna retains low profile even with the radome being

Table 2: Comparison of the proposed antenna array with previous works.

Refs	Operating bands (GHz)	Height (mm)	Size (mm^2/λ_0^2)	Isolation (dB)	Element gain (dB)	Efficiency	Cross-polarization (dB)	Radome integrated
[4]	3.3–3.6 8.7%	18.8 $0.216\lambda_0$	26×26 0.3×0.3	25	7.3	>89.3%	−17/−24.5	No
[5]	3.28–5.31 47.3%	10.5 $0.15\lambda_0$	96×96 1.37×1.37	37	6.3	>65.0%	−20	No
[16]	5.4–5.6 3.6%	5.3 $0.097\lambda_0$	19.5×16.8 0.36×0.31	25	9.5	—	−19.5	Yes
[17]	3.3–3.66 10.3%	5.813 $0.067\lambda_0$	80×80 0.93×0.93	35	8.2	—	−20.8	No
[18]	3.3–3.6 8.7%	6.8 $0.078\lambda_0$	25.2×25.2 0.29×0.29	26	8.5	—	−22	Yes
[19]	4.1–4.35 5.8–6.15 5.9%/5.9%	— — —	50×50 1×1	28 30	6.5	—	−25 −15	No
[20]	3.14–3.8 16.6%	11.8 $0.136\lambda_0$	82×82 0.95×0.95	43	8.1	>78%	−30	No
[25]	3.28–3.71 4.8–5.18 12.3%/7.6%	11.3 $0.13\lambda_0$	65×65 0.75×0.75	37	8.34	—	−18.2	No
[26]	3.12–3.9 22.2%	11.3 $0.15\lambda_0$	65×65 0.7×0.7	35.2	8.1	—	−21	No
[5]	3.26–3.73 4.68–5.05 13.5%/7.6%	9.5 $0.13\lambda_0$	96×96 1.34×1.34	25	9.1	>65%	−20	No
This work	3.3–6.0 58.1%	6.3 $0.097\lambda_0$	45×80 0.7×1.2	33	6.4	>65%	−30	Yes

considered, which makes the present design a potential base-station antenna.

4. Conclusion

A broadband dual-polarized antenna array covering the entire sub-6 GHz band is proposed. In the design of antenna element and array, the advantageous side of the dielectric radome is utilized, and a parasitic patch is etched on its inner surface, which greatly expands the bandwidth of the antenna. The use of differential feeding technique, square-shaped main and parasitic patches, and broadband feeding network maintains good symmetry of the antenna structure, resulting in very low cross-polarization level and high isolation between feeding ports within the entire frequency band. Experimental results verify the proposed design, and the antenna array may be a good candidate for base-station applications.

Data Availability

The data used to support the findings of this study are available from the corresponding author upon request.

Conflicts of Interest

There are no conflicts of interest regarding the publication of this paper.

References

[1] New frequency range for NR (3.3–4.2 GHz), 3GPP TR 38.813, 2017.

[2] New frequency range for NR (4.4–5 GHz), 3GPP TR 38.814, 2017.

[3] New frequency range for NR (24.25–29.5 GHz), 3GPP TR 38.815, 2017.

[4] H. Huang, X. Li, and Y. Liu, "5G mimo antenna based on vector synthetic mechanism," *IEEE Antennas and Wireless Propagation Letters*, vol. 17, no. 6, pp. 1052–1055, 2018.

[5] B. Feng, X. He, J.-C. Cheng, Q. Zeng, and C.-Y.-D. Sim, "A low-profile differentially fed dual-polarized antenna with high gain and isolation for 5G microcell communications," *IEEE Transactions on Antennas and Propagation*, vol. 68, no. 1, pp. 90–99, 2020.

[6] C. Ding, H.-H. Sun, R. W. Ziolkowski, and Y. Jay Guo, "A dual layered loop array antenna for base stations with enhanced cross-polarization discrimination," *IEEE Transactions on Antennas and Propagation*, vol. 66, no. 12, pp. 6975–6985, 2018.

[7] H. Zhu, Y. Qiu, and G. Wei, "A broadband dual-polarized antenna with low profile using nonuniform metasurface," *IEEE Antennas and Wireless Propagation Letters*, vol. 18, no. 6, pp. 1134–1138, 2019.

[8] L. H. Ye, X. Y. Zhang, Y. Gao, and Q. Xue, "Wideband dual-polarized two-beam antenna array with low sidelobe and grating-lobe levels for base-station applications," *IEEE Transactions on Antennas and Propagation*, vol. 67, no. 8, pp. 5334–5343, 2019.

[9] L.-H. Wen, S. Gao, Q. Luo et al., "A wideband differentially fed dual-polarized antenna with wideband harmonic suppression," *IEEE Transactions on Antennas and Propagation*, vol. 67, no. 9, pp. 6176–6181, 2019.

[10] L.-H. Wen, S. Gao, Q. Luo et al., "A compact wideband dual-polarized antenna with enhanced upper out-of-band suppression," *IEEE Transactions on Antennas and Propagation*, vol. 67, no. 8, pp. 5194–5202, 2019.

[11] L. Wu, R. Li, Y. Qin, and Y. Cui, "Bandwidth-enhanced broadband dual-polarized antennas for 2G/3G/4G and imt services," *IEEE Antennas and Wireless Propagation Letters*, vol. 17, no. 9, pp. 1702–1706, 2018.

[12] Y. Zhu, Y. Chen, and S. Yang, "Decoupling and low-profile design of dual-band dual-polarized base station antennas using frequency-selective surface," *IEEE Transactions on Antennas and Propagation*, vol. 67, no. 8, pp. 5272–5281, 2019.

[13] C. Wang, Y. Chen, and S. Yang, "Dual-band dual-polarized antenna array with flat-top and sharp cutoff radiation patterns for 2G/3G/lte cellular bands," *IEEE Transactions on Antennas and Propagation*, vol. 66, no. 11, pp. 5907–5917, 2018.

[14] Y. Liu, S. Wang, N. Li, J.-B. Wang, and J. Zhao, "A compact dual-band dual-polarized antenna with filtering structures for sub-6 GHz base station applications," *IEEE Antennas and Wireless Propagation Letters*, vol. 17, no. 10, pp. 1764–1768, 2018.

[15] Y. Cui, L. Wu, and R. Li, "Bandwidth enhancement of a broadband dual-polarized antenna for 2G/3G/4G and imt base stations," *IEEE Transactions on Antennas and Propagation*, vol. 66, no. 12, pp. 7368–7373, 2018.

[16] H. Li, L. Kang, F. Wei, Y.-M. Cai, and Y.-Z. Yin, "A low-profile dual-polarized microstrip antenna array for dual-mode oam applications," *IEEE Antennas and Wireless Propagation Letters*, vol. 16, pp. 3022–3025, 2017.

[17] L.-H. Wen, S. Gao, Q. Luo, Q. Yang, W. Hu, and Y. Yin, "A low-cost differentially driven dual-polarized patch antenna by using open-loop resonators," *IEEE Transactions on Antennas and Propagation*, vol. 67, no. 4, pp. 2745–2750, 2019.

[18] H. Huang, X. Li, and Y. Liu, "A low-profile, dual-polarized patch antenna for 5G mimo application," *IEEE Transactions on Antennas and Propagation*, vol. 67, no. 2, pp. 1275–1279, 2019.

[19] C.-X. Mao, S. Gao, Y. Wang et al., "Integrated dual-band filtering/duplexing antennas," *IEEE Access*, vol. 6, pp. 8403–8411, 2018.

[20] Y. Liu, S. Wang, X. Wang, and Y. Jia, "A differentially fed dual-polarized slot antenna with high isolation and low profile for base station application," *IEEE Antennas and Wireless Propagation Letters*, vol. 18, no. 2, pp. 303–307, 2019.

[21] Z. Tang, J. Liu, Y.-M. Cai, J. Wang, and Y. Yin, "A wideband differentially fed dual-polarized stacked patch antenna with tuned slot excitations," *IEEE Transactions on Antennas and Propagation*, vol. 66, no. 4, pp. 2055–2060, 2018.

[22] W. R. Eisenstadt, R. Stengel, and B. M. Thompson, *Microwave Differential Circuit Design Using Mixed Mode S-Parameters*, vol. 42–45, pp. 1–25, Artech House, Boston, MA, USA, 2006.

[23] Z. Wang, S. Fang, S. Fu, and S. Lv, "Dual-band probe-fed stacked patch antenna for GNSS applications," *IEEE Antennas Wireless Propagation Letters*, vol. 8, pp. 100–103, 2009.

[24] N. Seman and M. Bialkowski, "Microstrip-slot transition and its applications in multilayer microwave circuits," *Passive Microwave Components Antennas*, pp. 247–266, InTech, Rijeka, Croatia, 2010.

[25] Y. Li, Z. Zhao, Z. Tang, and Y. Yin, "Differentially fed, dual-band dual-polarized filtering antenna with high selectivity for 5G sub-6 GHz base station applications," *IEEE Transactions on Antennas and Propagation*, vol. 68, no. 4, pp. 3231–3236, 2020.

[26] Y. Li, Z. Zhao, Z. Tang, and Y. Yin, "Differentially-fed, wideband dual-polarized filtering antenna with novel feeding structure for 5G sub-6 GHz base station applications," *IEEE Access*, vol. 7, pp. 184718–184725, 2019.